REPORT DOCUMENTATION PAGE

Public Reporting burden for this collection of information is estimated to average 1 hour per response, including the time for reviewing instructions, searching existing data sources, gathering and maintaining the data needed, and completing and reviewing the collection of information. Send comment regarding this burden estimates or any other aspect of this collection of information, including suggestions for reducing this burden, to Washington Headquarters Services, Directorate for information Operations and Reports, 1215 Jefferson Davis Highway, Suite 1204, Arlington, VA 22202-4302, and to the Office of Management and Budget, Paperwork Reduction Project (0704-0188,) Washington, DC 20503.

1. AGENCY USE ONLY (Leave Blank)	2. REPORT DATE	3. REPORT TYPE AND DATES COVERED
		reprint, FY2007

4. TITLE AND SUBTITLE	5. FUNDING NUMBERS
Intrinsic bonding defects in transition metal elemental oxides	W911NF-04-D-0003

6. AUTHOR(S)

G. Lucovsky, H. Seo, L. B. Fleming, M. D. Ulrich, J. Lüning, et. al.

7. PERFORMING ORGANIZATION NAME(S) AND ADDRESS(ES) Dept of Physics, NCSU, Raleigh, NCS 27695-8202	8. PERFORMING ORGANIZATION REPORT NUMBER

9. SPONSORING / MONITORING AGENCY NAME(S) AND ADDRESS(ES) U. S. Army Research Office P.O. Box 12211 Research Triangle Park, NC 27709-2211	10. SPONSORING / MONITORING AGENCY REPORT NUMBER 48745.1-PH-SR

11. SUPPLEMENTARY NOTES

The views, opinions and/or findings contained in this report are those of the author(s) and should not be construed as an official Department of the Army position, policy or decision, unless so designated by other documentation.

12 a. DISTRIBUTION / AVAILABILITY STATEMENT Approved for public release; Federal Purpose Rights.	12 b. DISTRIBUTION CODE

13. ABSTRACT (Maximum 200 words)

Gate dielectrics comprised of nanocrystalline HfO_2 in gate stacks with thin SiO_2/SiON interfacial transition regions display significant asymmetries with respect to trapping of Si substrate injected holes and electrons. Based on spectroscopic studies, and guided by ab initio theory, electron and hole traps in HfO_2 and other transition metal elemental oxides are assigned to O-atom divacancies, clustered at internal grain boundaries. Three engineering solutions for defect reduction are identified: i) deposition of ultra-thin, < 2 nm, HfO_2 dielectric layers, in which grain boundary formation is suppressed by effectively eliminating inter-primitive unit cell π-bonding interactions, ii) chemically phase separated high HfO_2 silicates in which inter-primitive unit cell p-bonding interactions are suppressed by the two nanocrystalline grain size limitations resulting from SiO_2 inclusions, and iii) non-crystalline Zr/Hf Si oxynitrides without grain boundary defects.

14. SUBJECT TERMS oxides, defects, spectroscopy, electronic structure, gate dielectric	15. NUMBER OF PAGES 6
	16. PRICE CODE

17. SECURITY CLASSIFICATION OR REPORT **UNCLASSIFIED**	18. SECURITY CLASSIFICATION ON THIS PAGE **UNCLASSIFIED**	19. SECURITY CLASSIFICATION OF ABSTRACT **UNCLASSIFIED**	20. LIMITATION OF ABSTRACT **UU**

NSN 7540-01-280-5500

Standard Form 298 (Rev.2-89)
Prescribed by ANSI Std. 239-18
298-102

Enclosure 1

Intrinsic bonding defects in transition metal elemental oxides

G. Lucovsky[a,*], H. Seo[a], L.B. Fleming[a], M.D Ulrich[a,b], J. Lüning[c],
P. Lysaght[d], G. Bersuker[d]

[a] Department of Physics, North Carolina State University, Raleigh, NC 27695-8202, USA
[b] Army Research Office, Research Triangle Park, NC 27709-2211, USA
[c] Stanford Synchrotron Research Laboratory, Menlo Park, CA 94025, USA
[d] International Sematech, Austin, TX 78741, USA

Abstract

Gate dielectrics comprised of nanocrystalline HfO_2 in gate stacks with thin $SiO_2/SiON$ interfacial transition regions display significant asymmetries with respect to trapping of Si substrate injected holes and electrons. Based on spectroscopic studies, and guided by ab initio theory, electron and hole traps in HfO_2 and other transition metal elemental oxides are assigned to O-atom divacancies, clustered at internal grain boundaries. Three *engineering solutions* for defect reduction are identified: i) deposition of ultra-thin, < 2 nm, HfO_2 dielectric layers, in which grain boundary formation is suppressed by effectively eliminating inter-primitive unit cell π-bonding interactions, ii) chemically phase separated high HfO_2 silicates in which inter-primitive unit cell p-bonding interactions are suppressed by the two nanocrystalline grain size limitations resulting from SiO_2 inclusions, and iii) non-crystalline Zr/Hf Si oxynitrides without grain boundary defects.

1. Introduction

Densities of interfacial and bulk traps/fixed charge in high-k dielectrics are typically about one to two orders of magnitude higher ($\sim 10^{13}$ cm^{-2}) than in Si-SiO_2 devices. A crucial issue is to determine whether high-k defects are intrinsic and associated with the structure, nanocrystalline, non-crystalline, etc., or whether they are derived from processing, e.g., from chemical impurities. This paper presents spectroscopic studies of high-k gate dielectrics, with an emphasis on identification of electron and hole traps in gate stacks containing HfO_2 [1]. Asymmetry in hole and electron trapping represents a potentially significant limitation for the operation and reliability of CMOS circuits. Based on spectroscopic studies and ab initio molecular orbital (MO) theory, these differences in defect behavior are explained by different charge states of O-atom divacancy defects clustered at grain boundaries in nanocrystalline thin films prepared by remote plasma processing, RPECVD, reactive evaporation, RE, and atomic layer deposition, ALD. Spectroscopic studies have also been performed on nanocrystalline TiO_2, ZrO_2, HfO_2, and complex mixed oxides such as $ZrTiO_4$, $LaAlO_3$ and $La_2Ti_2O_7$, indicating qualitatively similar defects.

These grain boundary defects have been eliminated in several different ways: i) by limiting the size of nanocrystalline grains to < 2 nm by (a) limiting the dielectric film thickness to < 2 nm, and (b) limiting grain size in chemically phase separated silicates by SiO_2 inclusions, and ii) by deposition non-crystalline Zr/Hf Si oxynitrides without grain boundary defects; they are stable to temperatures of 1100°C, well above what is required for down-stream processing following gate film depositions. An emerging issue of importance is research into alternative dielectric for Ge and GaAs.

* corresponding author: lucovsky@ncsu.edu
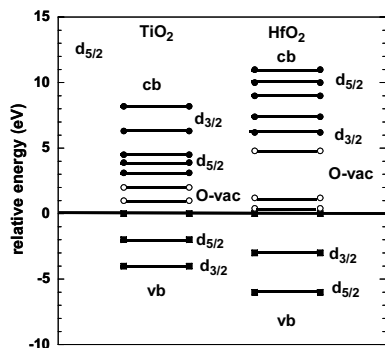Tel: +01 (919) 515 3301; Fax: +01 (919) 859 3191

Figure 1. Energy band of Ti/Hf elemental oxides. Valence (solid squares) and conduction band states (solid dots). Defects are indicated by open circles.
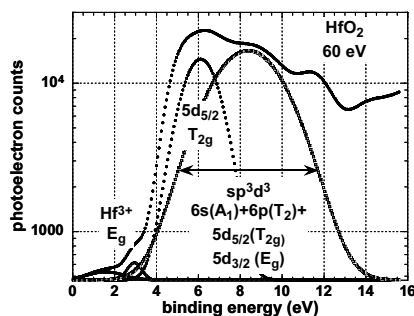

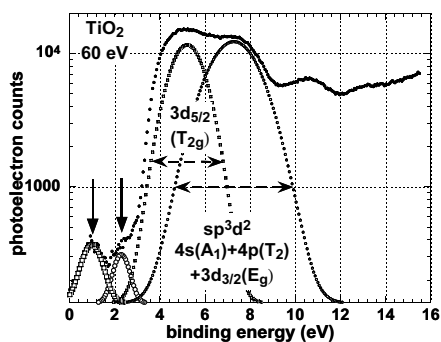Figure 2(a). SXPS valence band spectrum of HfO_2. 5d-state and defect features are identified.

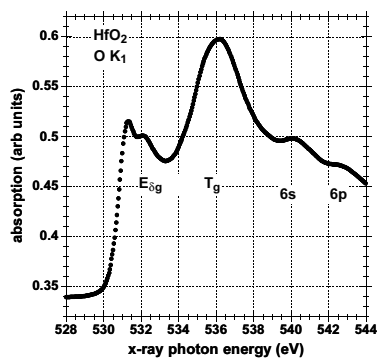Figure 2(b). SXPS valence band spectrum of TiO_2. 5d-state and defect features are identified.

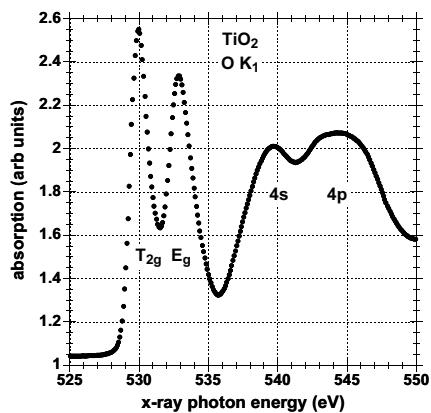Figure 3(a). O K_1 edge XAS spectrum of HfO_2. 5d-state features are identified.

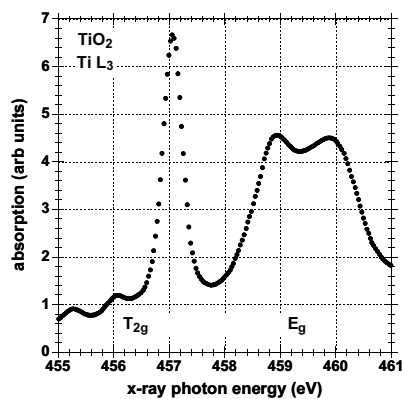Figure 3(b). O K_1 edge XAS spectrum of TiO_2. 3d-state features are identified.

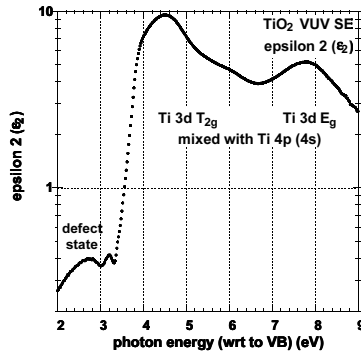Figure 4. Ti L3 edge XAS spectrum of TiO_2. Ti 3d J-T term split states are identified.

Figure 5(a). ε_2 spectrum from SE measurements for TiO_2. Ti 3d and defect state features are marked.

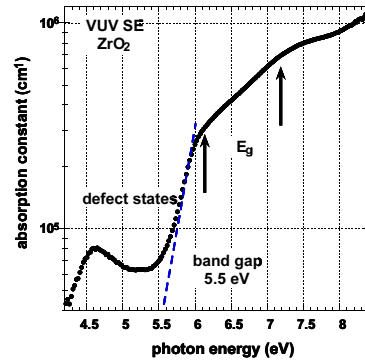Figure 5(b). ε_2 spectrum from SE measurements for ZrO_2. Zr 4d and defect state features are marked.
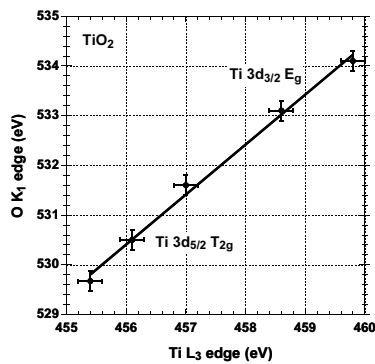
Figure 6(a). Plot of 3d-state energies from O K_1 XAS spectrum of TiO_2 versus 3-state energies from Ti L_3 XAS spectrum of TiO_2. The slope for this plot is 1.
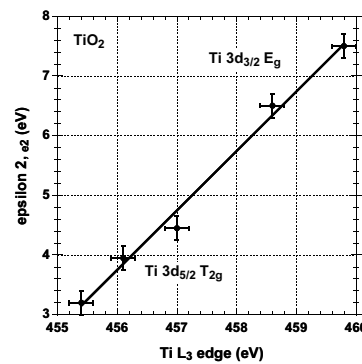
Figure 6(b). Plot of 3d-state energies from ε_2 spectrum of TiO_2 versus 3-state energies from Ti L_3 XAS spectrum of TiO_2. The slope for this plot is 1.
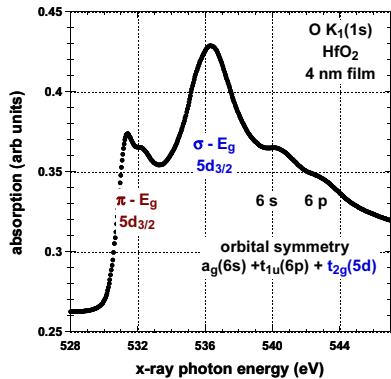
Figure 7(a). O K_1 edge XAS spectrum of HfO_2 for a film with a physical thickness of 4 nm. The two J-T contributions to band edge Hf $5d_{3/2}$ state are evident.
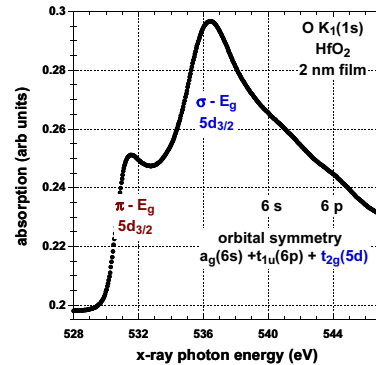
Figure 7(a). O K_1 edge XAS spectrum of HfO_2 for a film with a physical thickness of 2 nm. The band edge Hf $5d_{3/2}$ state appears a single feature with no J-T splitting.

2. Spectroscopic results and data reduction

Soft x-ray photoelectron spectroscopy (SXPS), near edge x-ray absorption spectroscopy (NEXAS), have detected defect states in nanocrystalline ZrO_2 and HfO_2 [2]. These spectra have been used to generate the energy level diagrams display in Fig. 1. This section of the paper address three different regions identified in Fig. 1: i) the electronic structure of the valence bands using HfO_2 and TiO_2 as examples of symmetry driven changes in transition metal (TM) d-states that derive from approximately cubic and octahedral coordination, ii) the electronic structure of TM conduction band states, and in particular the equivalence of TM d-state features for excitations from (a) localized O-atom non-bonding π-states at the top of the valence band, and (b) the localized O 1s core level state, and finally iii) intrinsic defect states within the forbidden bands that derive from O-atom vacancies that are clustered at nanocrystalline grain boundaries.

Figure 2 presents SXPS spectra for (a) HfO_2 and (b) TiO_2, each indicating the d-state features in the valence band, as well as occupied defect states above the respective valence band edges. Figure 3 presents O K_1 edge spectra for HfO_2 in 3(a) and TiO_2 in 3(b) indicating d-states, as well as s and p states features, that mirror those in the valence spectra of Figs. 2(a) and (b), respectively. The markers indicate Jahn-Teller term splittings of the respective crystal field split doublet and triplet E and T-symmetry d-states. Figure 4 gives the Ti L_3 spectrum for oxidations from the Ti $2p_{3/2}$ state to Ti 3d states. This spectrum also indicates five distinct that reflect the Jahn-Teller term splittings of the T_{2g} (triplet) and E_g (doublet) crystal field degenerate states. Figure 5 displays vis-VUV SE ε_2 spectra for TiO_2 and ZrO_2. [2]. These spectra indicates the energies of d-state features obtained by differentiation, as well as additional defect state features, ~1 to 3 eV below the respective d-state band edge features. Figure 5 includes plots the Jahn-Teller split d-state energies in the O K_1 spectrum for TiO_2, as a function of the energies of the corresponding d-state features in the TiO_2 (a) L_3 spectrum, and (4) the ε_2 spectrum derived from the SE studies. The plots in Figs. 6(a) and 6(b) each indicate a linear scaling relationship with slope of very nearly. At this stage of the paper, this is the basis for using d-state energies extracted from O K_1 edges of HfO_2 and ZrO_2, in combination with defect state features in the SXPS valence band and VUV SE ε_2 spectra, to locate energies of defect states within the forbidden energy gaps of TiO_2, ZrO_2 and HfO_2 as shown in Fig. 1. Analysis of spectroscopic data for ZrO_2 yields 4d-state and defect state features with only relative small shifts, ~0.2-0.4 eV, in energy with respect to the valence and conduction band edges as for HfO_2. As an example, photoconductivity (PC) and cathodo-luminescence

spectra support the intrinsic character of these defect.

3. Discussion

Electrical measurements on metal-oxide semi-conductor capacitors (MOSCAPs) by our group [3], yield the same asymmetric trapping as disclosed in Ref. 1. In summary, the analysis of electronic data, e.g., capacitance-voltage, C-V, and current-voltage, J-V, indicate: i) relatively shallow electron traps, ~0.5 eV below the conduction band edges of HfO_2 and ZrO_2, as well as ii) deep hole traps below the valence band edge of Si; ~ 3 eV above the HfO_2 valence band.

The spectroscopic measurements described above indicate electronic structure that is consistent with the local character of the Ti, Zr and Hf, 3d, 4d and 5d states making strong contributions to: i) the valence band, ii) the conduction band, and iii) the defects within the forbidden energy gap. These states are mixed with O-atom 2p σ- and 2p π-states. The states at the top of the valence band are always derived from O non-bonding π-states independent of the bonding geometry and symmetry of the transition metal atom. More detailed discussions of the energy band structure of octahedral and tetrahedral bonding of group IVB TMs, Ti, Zr and Hf, to O are presented in Refs. 3, 4 and 5. These references address the differences in crystal field d-state splittings for octahedral and tetrahedral coordination, and include the extension to cubic coordination as well. Reference 5 provides particularly good insight in the separation of the valence band states into π- and σ-bonding contributions, highlighting the π-bonding contributions at the top of the valence and their atomic parentage, TM d-states, T_{2g} for octahedral coordination, and E_g for tetrahedral coordination, and contrasting this with hybridisation or mixing atomic TM states for σ-bonding, e.g., a mixture of Ti 4s, 4p(σ) and $3d_{3/2}$ or E_g states for octahedrally-coordinated Ti, and a equivalent mixture $4s + 4p + 5d_{5/2}$ or Tg for the 7-fold coordination of monoclinic ZrO_2. As noted above, the conduction band or final states for optical transitions mirror the valence band structure. The spectral resolution and intrinsic line-widths of these final states make it possible to identify the J-T term split states that derive from departures from ideal octahedral, tetrahedral and cubic bonding [4,6]. For Ti and Sc, the core hole life-times in 2p atomic states are sufficiently long to resolve both crystal field and Jahn-Teller splittings in the 3d states in the L_3 spectrum, whilst for Zr and Hf, the core life-times are significantly shorter, and it is not possible to resolve J-T split states in either ZrO_2 or HfO_2; in these oxides, as noted above, these splittings can be extracted from O K_1 edge spectra by differentiation.
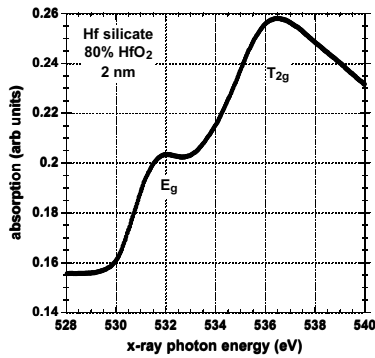
The nature of the intrinsic nanocrystalline defects

Figure 8(a). O K$_1$ edge XAS spectrum of a 2nm phase separated Hf silicate film. The band edge Hf 5d$_{3/2}$ is single feature with no J-T splitting.
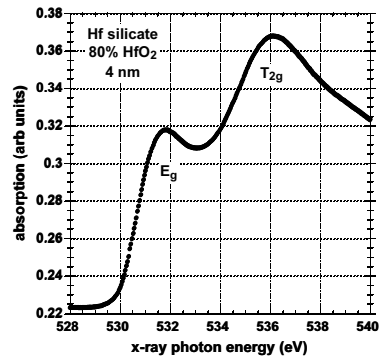

Figure 8(a). O K$_1$ edge XAS spectrum of a 4nm thick phase separated Hf silicate film. The Hf 5d$_{3/2}$ feature is is stronger than in the 2nm film, but with no J-T splitting.
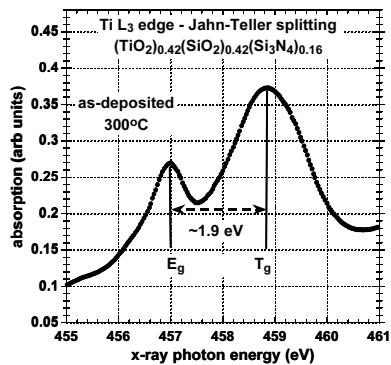

Figure 9(a). Ti L$_3$ spectrum for a low, 16% Si$_3$N$_4$ Ti Si oxynitride, as-deposited. The E$_g$ - T$_g$ slitting of < 2eV is indicates 4-fold tetrahedral bonding of Ti to O-atoms.
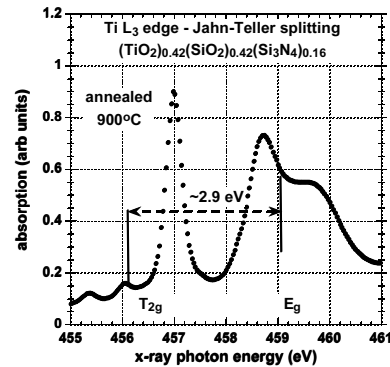

Figure 9(b). Ti L$_3$ spectrum for a low, 16% Si$_3$N$_4$ Ti Si oxynitride, 900°C anneal. The 5 E$_g$ and T$_g$ features are indicative of a 6-fold octahedral bonding of Ti to O-atoms
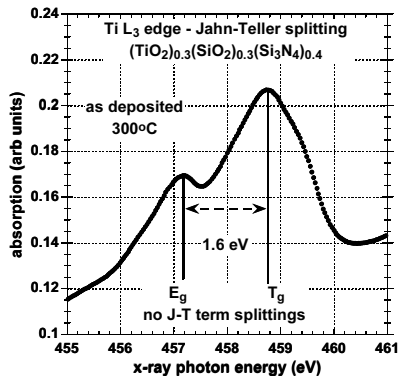

Figure 9(c). Ti L$_3$ spectrum for a high, 42% Si$_3$N$_4$ Ti Si oxynitride, as-deposited. The E$_g$ - T$_g$ slitting of < 2eV is indicates 4-fold tetrahedral bonding of Ti to O-atoms.
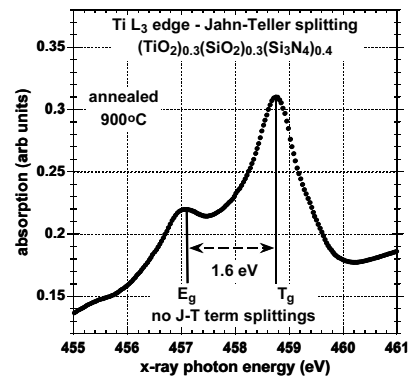

Figure 9(d). Ti L$_3$ spectrum for a high, 42% Si$_3$N$_4$ Ti Si oxynitride, 900°C anneal. The E$_g$ - T$_g$ slitting of < 2eV is indicates 4-fold tetrahedral bonding of Ti to O-atoms.

has been identified by comparing ab initio calculations for octahedrally coordinated Ti^{4+} atoms in TiO_2 with Ti^{3+} in $Ti(H_2O)_6^{3+}$ clusters and Ti_2O_3 [3] The defect electronic structure is *consistent with* electron transfer from a Ti-atom of a divacancy into two *vacant* O-atom sites. These comparisons include crystal field splittings, but neglect of E_g and T_{2g} state degeneracy removal by Jahn-Teller (J-T) distortions. The inherent properties of the divacancy defects are: i) electronic states of Ti^{3+} fall that within the energy gap of the Ti^{4+}-O bonding in TiO_2, ii) relative energies that are not changed by J-T splitting of the TiO_2 states, iii) partially-occupied T_{2g} states at the valence band edge with degeneracy lifted by a local J-T distortion, and iv) unoccupied E_g states at the conduction band edge with the degeneracy lifted. The T_{2g} states of Ti^{3+} are occupied and act as traps for substrate hole injection, whilst E_g states are empty, and act as traps for substrate trapping states for transport, e.g., substrate electron injection [1], and band edge photoconductivity [7].

Similar energy level diagrams apply to differences between the Zr(Hf) and $Zr(Hf)^{3+}$ and $Zr(Hf)^{4+}$ states in divacancies and bulk $Zr(Hf)O_2$, respectively. The primary difference between the Ti^{3+} and $Zr(Hf)^{3+}$ defects is the symmetry of the d-states. The occupied states for $Zr(Hf)^{3+}$ are J-T term-split E_g states, and empty states are J-T term split T_g states.

4. Engineering solutions for defect elimination

Three *materials engineering solutions* for elimination of these intrinsic defects are presented. One involves suppression of defect states in ultra-thin (< 2nm) HfO_2 layers by suppressing intra-primitive unit cell π-bonding interactions that couple Hf-atom 5d p states in one primitive cell with Hf atoms in at least two neighboring primitive cells [8]. The length scale for this is ~ 1.5-2.0 nm. The second is by chemically phase separation high HfO_2 content silicates by annealing at temperatures >700°C. In the instance, the inter-primitive unit cell π-bonding interactions are suppressed by the nanocrystalline grain size limitations resulting from SiO_2 inclusions. The third is by direct deposition of non-crystalline Ti, Zr and Hf Si oxynitride alloys, $(Ti/Zr/Hf)O_2)_x(SiO_2)_y(Si_3N_4)_{1-x-y}$, that are Si_3N_4 rich: x~y ≈ 0.3-0.32 and 1-x-y ≈ 0.36-0.4 [9].

Consider the first class of materials. The O K_1 edge spectra in Figs. 7(a) and 7(b) indicate a marked difference between the lowest $5d_{3/5}$ (E_g) π-states. A J-T term splitting is clearly evident in Fig. 7(a) for the 4 nm thick sample, but this is not the case for the spectrum in Fig. 7(b) for the 2 nm film. Suppression of the J-T term splittings indicates a decoupling between the $5d_{3/2}$ π-states in nearest neighbor primitive unit cells. This is accompanied by a broadening the band edge spectral feature, which renders the band edge grain boundary traps inactive.

Figures 8(a) and (b) compare the O K_1 spectra for two Hf silicate alloys with 80% HfO_2 and 20% SiO2 after annealing at 700°C. In each case the J-T splitting of the band edge E_g state is suppressed by the nature of the thin film morphology; SiO_2 inclusions that (a) limit nanocrystalline grain size to < 2m in films that are 2 nm, as well as 4 nm thick, , but (b) can not suppressing a narrowing the O K_1 edge feature when the film thickness is increases from 2 nm to 4 nm.

Studies of O K_1 and N K_1 edges of Zr Si oxynitrides indicate 4-fold coordinated Zr with O nearest-neighbors, and Si, O and N bonding similar to Si_2ON_2 Zr/Hf Si oxynitride alloys are stable against phase separation up to 1100°C. The dependence on the Si_3N_4 content is illustrated in Figs. 9(a), (b), (c) and (d) for Ti Si oxynitrides. For the low Si_3N_4 Ti Si oxynitride, $(TiO_2)_{0.16}(SiO_2)_{0.42}(Si_3N_4)_{0.42}$, the Ti atom coordination, obtained from d-state crystal field and/or term splittings is four as deposited, and increases to six after chemical phase separation that includes SiO_2 and nanocrystalline TiO_2. In contrast, the coordination is four, for an as-deposited and annealed (900°C) Ti Si oxynitride with 40% Si_3N_4, and equal concentrations of TiO_2 and SiO_2, ~ 30%

Electrical measurements indicate that ultra-thin HfO_2 annealed in N_2 or NH_3 at 700°C, and Zr/Hf Si oxynitrides can be scaled to EOT values to 0.7-0.8 nm, and extending scaling past the 0.45 nm node [8].

References

[1] Zu X, Houssa M, DeGendt S and Hyens M. Appl. Phys. Lett.80 (2001) pp. 1975-1978.

[2] Lucovsky G et. al. IEEE Trans. Dev. Mat. Reliability 5 (2005), pp. 65-84.

[3] CJ Ballhausen and HB Gray, *Molecular Orbital Theory* (Benjamin, New York, 1964); HB Gray, *Electrons and Chemical Bonding* (Benjamin, New York, 1965).

[4] PA Cox, *Transition Metal Oxides* (Clarendon, Oxford, 1992)

[5] FA Cotton, Chemical Applications of Group Theory, (Wiley Interscience, New York, 1963).

[6] I.B. Bersuker, *Electronic structure and properties of transition metal compounds: introduction to the theory* (Wiley, New York, 1996); *The Jahn-Teller effect* (Cambridge University Press, Cambridge, 2006).

[7] Lucovsky G and Lüning J. Proceedings of ESSDERC 2005 Grenoble France (2005), pp. 439-444.

[8] Kirsch PD et al. Proceedings of ESSDERC 2005 Grenoble France (2005), pp. 367-370.

[9] Ju B. Properties of Zr-Si Oxynitride Dielectric Alloys. PhD. Thesis, NC State University, Raleigh USA 2000.